ACS APPLIED MATERIALS & INTERFACES

www.acsami.org

Research Article

Waste- and Cd-Free Inkjet-Printed Zn(O,S) Buffer for Cu(In,Ga)(S,Se)$_2$ Thin-Film Solar Cells

Van Ben Chu,* Daniel Siopa, Alice Debot, Damilola Adeleye, Mohit Sood, Alberto Lomuscio, Michele Melchiorre, Jérôme Guillot, Nathalie Valle, Brahime El Adib, Jonathan Rommelfangen, and Phillip J. Dale*

Cite This: *ACS Appl. Mater. Interfaces* 2021, 13, 13009−13021

Read Online

ACCESS | Metrics & More | Article Recommendations | Supporting Information

ABSTRACT: Thin film semiconductors grown using chemical bath methods produce large amounts of waste solvent and chemicals that then require costly waste processing. We replace the toxic chemical bath deposited CdS buffer layer from our Cu(In,Ga)(S,Se)$_2$ (CIGS)-based solar cells with a benign inkjet-printed and annealed Zn(O,S) layer using 230 000 times less solvent and 64 000 times less chemicals. The wetting and final thickness of the Zn(O,S) layer on the CIGS is controlled by a UV ozone treatment and the drop spacing, whereas the annealing temperature and atmosphere determine the final chemical composition and band gap. The best solar cell using a Zn(O,S) air-annealed layer had an efficiency of 11%, which is similar to the best conventional CdS buffer layer device fabricated in the same batch. Improving the Zn(O,S) wetting and annealing conditions resulted in the best device efficiency of 13.5%, showing the potential of this method.

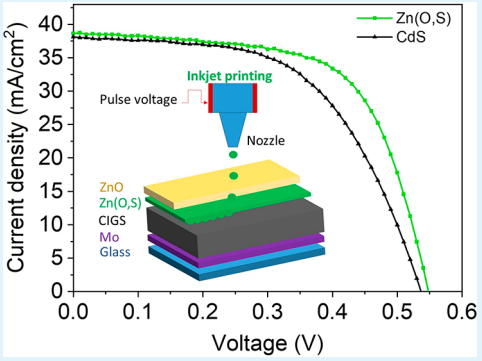

KEYWORDS: *inkjet printing, Zn(O,S) buffer, thin film, CIGS solar cells, UV ozone, drop spacing*

INTRODUCTION

Thin-film inorganic solar cells require a buffer layer to achieve a high light to electric power conversion efficiency (PCE). Typically, a 50 nm n-type CdS thin film deposited by chemical bath deposition (CBD) technique is used as a buffer layer for both CdTe[1,2] and Cu(In,Ga)(S,Se)$_2$ (CIGS)[3] thin film solar cells. For CIGS devices CBD buffer layers fulfill a number of functions: (i) they provide pinhole free coverage of the rough absorber surfaces with only tens of nanometer thin films,[4−6] (ii) they modify the surface chemistry of the absorber surface,[7,8] (iii) they protect the absorber layer from sputter damage during the deposition of the window layers (e.g., ZnO, (Mg,Zn)O, ITO),[9,10] (iv) they provide a better lattice matching between absorber and window layer[11] and (v) they result in a high interface band gap that reduces interface recombination.[12,13] However, CdS detrimentally absorbs solar irradiation above 2.4 eV reducing the device short circuit current and power conversion efficiency (PCE),[14] it is toxic, and the normal CBD process produces a large concentrated volume of waste that must be safely disposed. Therefore, we investigate the inkjet printing of Zn(O,S) buffer layers for CIGS solar cells because these absorb less light and are less toxic and the deposition process uses minuscule amounts of solvent, and a virtually waste-free process.

Alternative buffer materials to CdS, which are environmentally benign and have larger band gaps, are desirable for thin film solar cells. Recently, Nakamura et al. reported a CIGS solar cell with a Zn-based buffer layer achieving a record PCE of 23.35%.[15] Zn(O,S) could be an ideal CdS alternative because of its tunable wide band gap of between 2.7 and 5.15 eV[16−18] and because it consists of only nontoxic elements. Zn(O,S) was investigated intensively for application in photovoltaics and optoelectronics using various deposition techniques. For example, Zn(O,S) was deposited by CBD technique,[19,20] atomic layer deposition (ALD),[21] sputtering,[22] spray pyrolysis,[23] chemical vapor deposition,[24] and sol−gel methods.[25] The CBD method is widely used to deposit Zn(O,S) buffer layer for CIGS thin film solar cells; however, the Zn(O,S) buffer formed by CBD usually consists of zinc oxide (ZnO) and zinc sulfide (ZnS) with zinc hydroxide (Zn(OH)$_2$) with Zn(OH)$_2$ on the top surface.[26] The Zn(OH)$_2$ acts as a barrier for transporting of charge carriers generated in the CIGS layer due to the large conduction band offset.[27] Consequently, CIGS solar cells with a CBD-Zn(O,S) buffer layer are generally less efficient than CIGS solar cells with a CdS buffer layer.[19]

Received: September 18, 2020
Accepted: February 1, 2021
Published: March 9, 2021

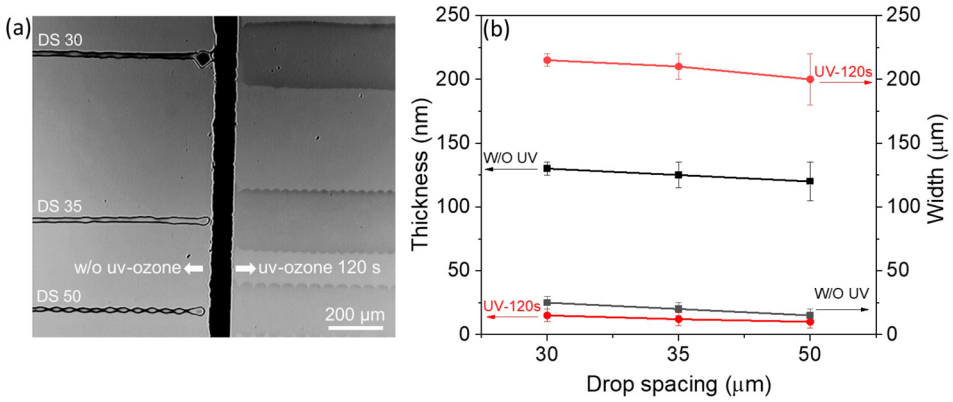

Figure 1. Effect of UV ozone on the printing of Zn(O,S) lines on a Mo substrate. The optical microscope image (Figure 1a) shows the printed Zn(O,S) lines with drop spacing of 30, 35, and 50 μm on non-UV-ozone-treated Mo (the left part) and 120 s UV-treated Mo (the right part). The thickness and width of the printed lines with different drop spacing and with and without UV ozone treatment on Mo substrates are shown in the Figure 1b.

Both CBD CdS and Zn(O,S) are atomically wasteful. This is because the CBD method relies on large volumes of liquid to ensure uniform chemical concentration and temperature within the deposition vessel. Typically, the volume of the CBD vessel is many times the volume of the solar cell substrates to avoid chemical or temperature gradients. The vessel volume must be heated for many minutes to aid the deposition process. After the buffer layer is deposited, the leftover solution is normally disposed of because it contains undesired waste products and is difficult to reuse. Additionally, the reaction vessel requires cleaning, typically using concentrated acids, which also requires subsequent neutralization and disposal. All these factors make finding an alternative buffer deposition technique desirable.

An atomically efficient solution based deposition method is inkjet printing and annealing, which splits the deposition and thin film formation into two separate parts. In the first part, a precursor ink stored in a closed 1.5 mL cartridge generates picoliter drops, which fall and wet the surface of the absorber layer around room temperature. In the second part, the wet layer is heated to evaporate the solvent, combust or pyrolyze unwanted surface tension and viscosity modifiers, and drive the reaction of the precursors to form the desired thin film. Advantageously, the closed cartridge limits the ink exposure to the environment, enables tens to hundreds of depositions, and can be used months later. The small droplet size means that no chemicals and solvent are wasted, and that there is no cleanup required of large reaction vessels. Care is required to formulate the precursor ink with the correct surface tension and viscosity so that it is jettable in a controllable manner and that it wets the surface of the substrate well.[28] Inkjet printers can be easily integrated into an in-line or a vacuum-line fabrication process which help to scale up industrial production. It is a contactless and accurate deposition technique, allowing the patterning of thin films without masks. It provides the ability to flexibly design the materials and structures on a single substrate. Additionally, the thickness of the deposited thin film is easily tuned by either changing the drop spacing, the nozzle size, the jetting voltage, or the number of printed layers or the concentration of the precursor materials in the inks.

Several groups used inkjet printing to deposit continuous[29] and patterned thin films.[30,31] Other groups used inkjet printing to deposit functional materials. For example, Hoth et al. printed photoactive material for organic solar cells and achieved an efficiency of 3.5%,[32] Li et al. printed perovskite solar cells and achieved an efficiency of 19.6%,[33] and Lin et al. printed CIGS absorber layers and achieved a device efficiency of 11.3%.[34] Despite the advantages of inkjet printing, we could find no report on the inkjet printing of Zn(O,S) buffer layers for CIGS thin film solar cells.

One key aspect of printing uniform films is that the ink must conformally wet the surface of the substrate that it is being deposited onto. UV-ozone treatment can be used to improve the wettability of surfaces.[35] The effect of UV-ozone treatment on inorganic thin film semiconductors is scarcely known. Recently, van Maris et al.[36] found that after 90 s of treatment on an industrial CIGS surface, carbonaceous species had dropped to one-third of the initial amount, but they also detected the presence of indium, sulfur, and selenium oxides. These species could be expected to be detrimental to the device performance because aging absorbers in air is known to lower their quasi-Fermi level splitting.[37] Nonetheless, UV-ozone treatment has been reported as a fast, simple, and effective method for surface passivation of kesterite films and boosted the performance of solar cells.[38]

Here, we report on inkjet-printed and annealed Zn(O,S) thin films and applied them to CIGS thin-film solar cells. Initially, the Zn(O,S) layers were printed and annealed on molybdenum, quartz, or silicon wafer substrates to easily investigate the morphology, crystal structure, composition, and optical properties without interference from a CIGS substrate. The printed precursor films require post annealing to evaporate the solvents and convert the wet precursor layers to solid semiconductor thin films by decomposition and/or combustion reactions at elevated temperature. The temperature of this annealing step might affect the Zn(O,S) properties and the underlying CIGS absorber layer when applied to solar cells. Therefore, we investigated the effect of annealing temperature on the properties of the Zn(O,S) films and the performance of solar cell devices. To understand the benefits of printed Zn(O,S) films as buffer layers for CIGS solar cells, we compared the performance of these solar cells with those of CBD-CdS buffer layers while keeping all other device layers the same.

https://dx.doi.org/10.1021/acsami.0c16860
ACS Appl. Mater. Interfaces 2021, 13, 13009−13021

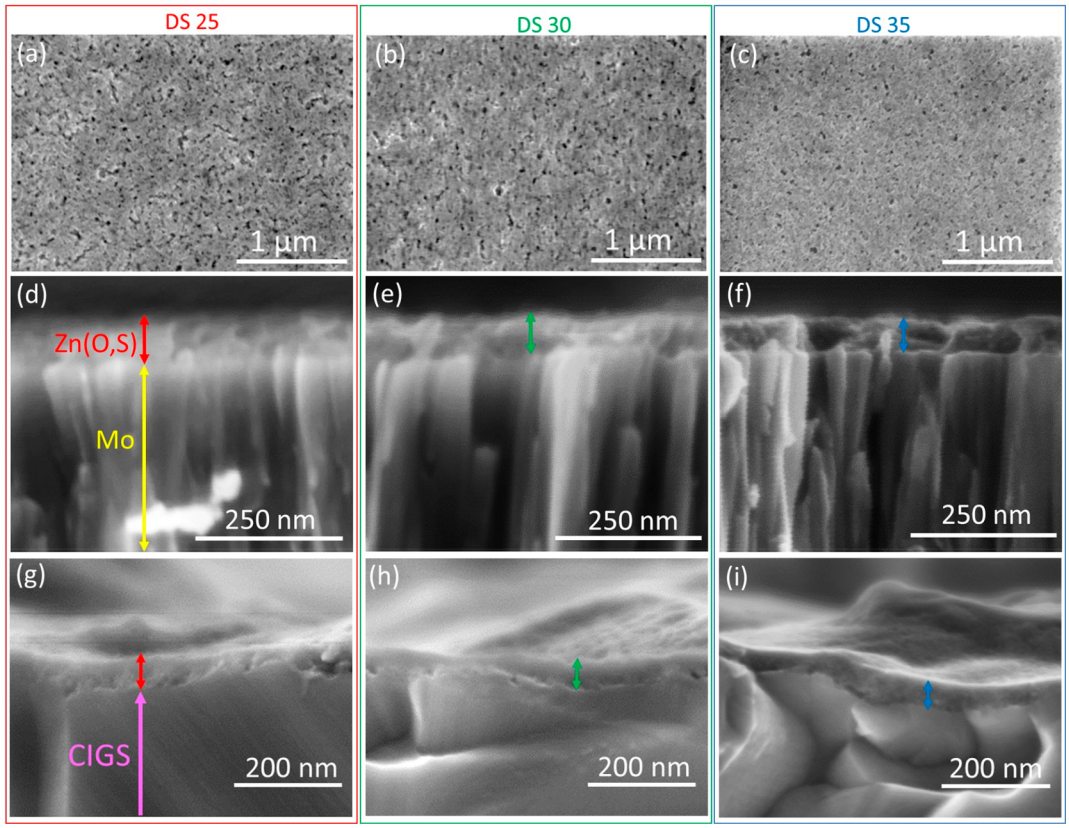

Figure 2. (a–c) Top-view and (d–f) cross-sectional view SEM images of Zn(O,S) films printed and air-annealed at 250 °C for 10 min on Mo substrates with drop spacing of 25, 30, and 35 μm, respectively. (g–i) Cross-sectional SEM images showing the coverage of printed Zn(O,S) on CIGS films. The red, green, and blue vertical arrows denote the Zn(O,S) film printed at different drop spacing.

RESULTS AND DISCUSSION

To investigate the ink wetting, morphology, and thickness of the Zn(O,S) films, we printed Zn(O,S) films on a low roughness Mo substrate with different drop spacings, which is the distance between two ejected drops. Depositing drops closer together should form a thicker Zn(O,S) film. To improve the wettability, we treated the Mo surface with UV ozone to remove any organic residues and also increase the surface energy.[39] Figure 1a is an optical microscope image with three printed Zn(O,S) lines a single drop wide, with increasing drop spacing from top to bottom on untreated Mo, left, and UV-ozone-treated, right. The thickness and the width of the lines were measured using a profilometer and are plotted in the Figure 1b. On the untreated side, the lines with a drop spacing (DS) of 30 and 35 μm are straight with around 25 ± 5 μm width, whereas the 50 μm drop spacing line comprises a series of bulges with a maximum width of 30 μm and a minimum width of 10 μm. The thicknesses of the lines on untreated Mo on the left part were all in the range of 120 ± 15 nm. On the UV-ozone-treated part, the drops wet the substrate significantly better and have a line width of around 200 ± 20 μm with a slight corrugation, and thicknesses of 15 ± 5 nm. From these initial experiments, we conclude that UV ozone treatment is necessary to form continuous films of suitable thickness for the buffer layer application.

After printing the films, they have to be annealed to remove the solvent and unwanted components, as well as to form and crystallize the Zn(O,S). To investigate the morphology of the annealed Zn(O,S) thin films and to elucidate the relationship between drop spacing and final film thickness, we took top-view and cross-sectional SEM images of 250 °C air-annealed Zn(O,S) films printed on molybdenum substrates with drop spacings of 25 (a, d), 30 (b, e) and 35 μm (c, f), respectively, and show them in Figure 2. All the films show surface porosity with openings of around 50 nm in diameter dispersed evenly over the surface, with the smallest drop spacing showing the most, and the largest drop spacing the least. From the surface images it is unclear if these openings extend through to the substrate. The cross-sectional SEM images appear to show that all the films are compact and uniformly cover the top of the Mo. The Zn(O,S) films were also printed on CIGS to investigate the coverage on the absorbers. Figure 2g–i shows the cross-sectional SEM image of Zn(O,S) films, revealing a compact buffer thin film covering the CIGS absorbers. Atomic force microscopy imaging (see Figure S1) of the Zn(O,S) films printed on CIGS absorbers shows the absence of voids in the buffer layers. We choose the films printed on the smooth Mo surface to measure a nominal thickness of film for each drop spacing rather than those printed on the rougher CIGS surface. The cross-sectional thicknesses of the Zn(O,S) films were 68, 50, and 42 nm for drop spacings of 25, 30, and 35 μm, respectively. We can compare these experimental thicknesses to a theoretical thickness if we assume the ejected drop volume is 1 pL and the number of drops per unit area corresponding to the drop spacing. Table 1 shows the number of drops required to cover a 1 in. square surface and the measured and estimated thicknesses of the Zn(O,S) films printed with different drop spacing. The relative agreement between the measured and theoretical thicknesses is close, so we suppose that the films are

https://dx.doi.org/10.1021/acsami.0c16860
ACS Appl. Mater. Interfaces 2021, 13, 13009–13021

Table 1. Number of Drops and Volume of Ink to Print 1 in. × 1 in. Substrate and the Thickness of Zn(O,S) Films Printed with Drop Spacing of 25, 30, and 35 μm

drop spacing (DS)	DS 25	DS 30	DS 35
no. of drops	1 034 289	719 104	528 529
estimated ink volume (μL)	1.03	0.72	0.53
estimated thickness (nm)	72	50	37
thickness from SEM (nm)	68 ± 6	50 ± 6	42 ± 6

relatively compact and that most of the impurities have been removed.

Taking this analysis one step further we can compare the volume of ink used in inkjet printing to that used in the chemical bath deposition (CBD) method to cover the same surface area with a buffer layer. For example, to cover the whole area of a 1 in. square sample, the number of drops when printing with a drop spacing of 35 μm was 528 529 drops, which is ~0.53 μL of ink. To compare with the chemical bath deposition method in the laboratory scale, each bath needs 500 mL of solvent to deposit buffer layers for four samples with a size of 1 in. square.[40] The ink volume needed to deposit on the same area using inkjet printing is 2.2 μL. This is 230 000 times less solvent needed to deposit buffer layers on the same area than the CBD method. In addition, the mass of precursors used to deposit on the same area is 64 000 times lower than that of the CBD method.[41] This huge reduction in solvent and precursor usage would have a significant impact on the environment.

Grazing-incidence X-ray diffraction (GIXRD) was conducted to investigate the crystal structure of inkjet-printed and air-annealed Zn(O,S) films on Mo substrates at 200, 250, and 300 °C. To obtain a reasonable signal-to-noise ratio, we chose a thicker than normal layer of 200 nm thickness. The GIXRD (Figure 3) shows very broad peaks for all the samples

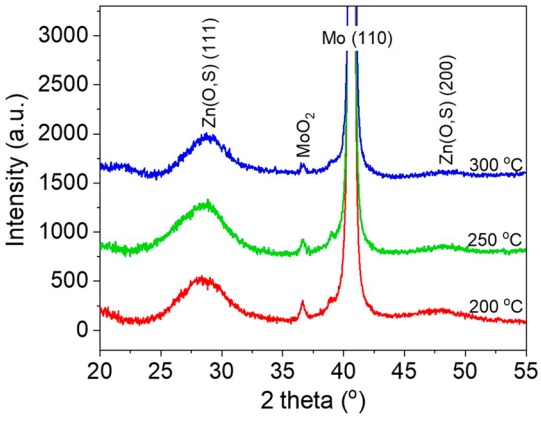

Figure 3. Grazing-incidence XRD patterns of Zn(O,S)/Mo films annealed at 200, 250, and 300 °C on a hot plate in air for 10 min. A small amount of MoO_2 is observed because of the oxidation process.

that match with the JCPDS No. 65−1691 referenced data of the cubic zinc blende structure of ZnS,[42,43] where the prominent peak varies from 28.3 to 28.8° 2θ (Figure S2), which is ascribed to the (111) planes. This is in agreement with Krunks et al., who for bulk powder samples formed from the same precursor compounds also found the zinc blende structure for annealing conditions of between 200 and 300 °C,[44] and Offor et al., who used chemical spray pyrolysis to synthesize ZnS using the same precursor materials.[45] This differs from the chemical bath deposition, which found both zinc blende and wurtzite structures,[46] whereas for ALD, the presence of the zinc blende structure could not be ruled out.[21] Here, the lattice constants of the cubic Zn(O,S) films are calculated to be 0.542, 0.546, and 0.536 nm for the 200, 250, and 300 °C annealed films, respectively (see Table S1), in good agreement with the pure ZnS cubic zinc blende structure, which has a reported lattice constant of 0.542 nm.[47,48] This suggests our films contain little oxygen.

The prominent peaks of the Zn(O,S) films are broad with the full width at half-maximum (fwhm) varying from 0.054 to 0.068 rad. From Debye−Sherrer's equation, with a shape factor of 0.9, the crystallite coherence length was estimated to be between 2.1 and 2.6 nm (Table S1), which is similar to that of ZnS nanoparticles synthesized with a sol−gel method as reported by Raleaooa et al.[42] This crystal coherence length is rather small but explains why virtually compact layers are observed, as the small crystals can pack well together. It reveals that grain growth under the present annealing conditions is limited.

The printed precursor films are required to be annealed at elevated temperatures to remove the solvents in the inks and form the Zn(O,S) phase itself. The exact annealing temperature may affect the composition and thus the optoelectronic properties of the Zn(O,S) films. Krunks et al. investigated the thermal decomposition of a $ZnCl_2$-thiourea ($Zn(tu)_2Cl_2$) complex by thermal gravimetric analysis both in air and in nitrogen and they found no mass loss below 200 °C[44] indicating the formation of Zn(O,S) from sintering the complex would be above this temperature.

Therefore, we investigated the optical properties of Zn(O,S) films air annealed between 200 and 300 °C. Figure 4a shows the optical transmission of the Zn(O,S) films on quartz substrates, along with the quartz substrate itself for comparison. The transmission of all the films is higher than 85% in the visible region. By increasing the annealing temperature, the transmission rises and the absorption edge shifts to longer wavelengths, meaning the bandgap of the Zn(O,S) film is reduced. Figure 4b shows a Tauc plot for a direct band gap. The bandgap of a Zn(O,S) film annealed at 200 °C is estimated to be 4.19 eV and the band gaps of Zn(O,S) films annealed at 250 and 300 °C are 4.08 and 3.78 eV, respectively. Similarly high band gaps of Zn(O,S) have been observed in the spray pyrolysis deposition method using the same precursor materials.[45] It is known that the bandgap of Zn(O,S) is correlated with the S/(O+S) atomic ratio, the local bonding arrangement due to crystallinity, and any bonding distortion due to lattice mismatch.[49] The high band gap of the Zn(O,S) annealed at low temperature might be due to quantum confinement, because diffraction measurements showed the films consist only of nanometer-sized particles. Supporting this argument, Deepak et al. found that the optical band gap of the Zn(O,S) correlated with the crystallite size and chemical composition in the film.[18]

To see if the observed band gap is changing due to the S/(O+S) ratio, we used X-ray photoelectron spectroscopy (XPS) to investigate the elemental composition of the films annealed at the three different temperatures. The XPS survey spectra of Zn(O,S) films annealed at 200−300 °C (Figure S3) appear to be similar except for the peak intensities. The Zn(O,S) films contain zinc, sulfur, and oxygen as expected but also chlorine, carbon, and nitrogen, which indicates incomplete removal of

https://dx.doi.org/10.1021/acsami.0c16860
ACS Appl. Mater. Interfaces 2021, 13, 13009−13021

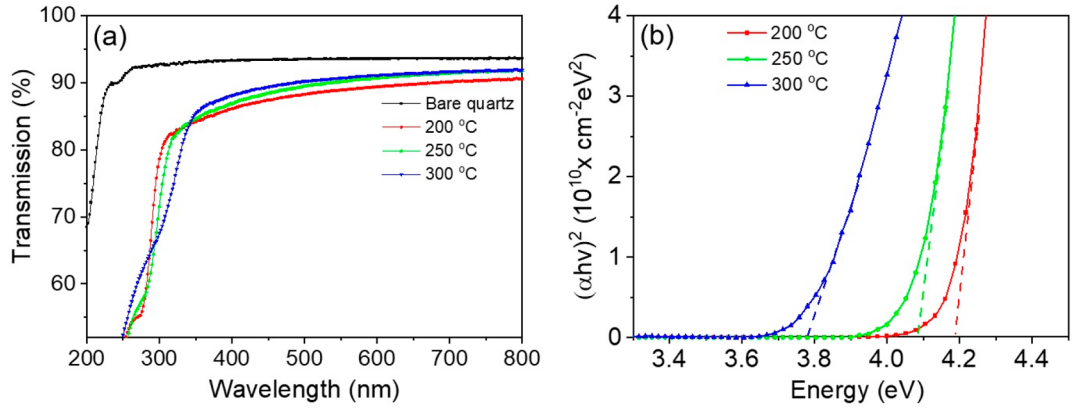

Figure 4. Zn(O,S)/quartz substrates air annealed at different temperatures: (a) transmission and (b) direct band gap tauc plots.

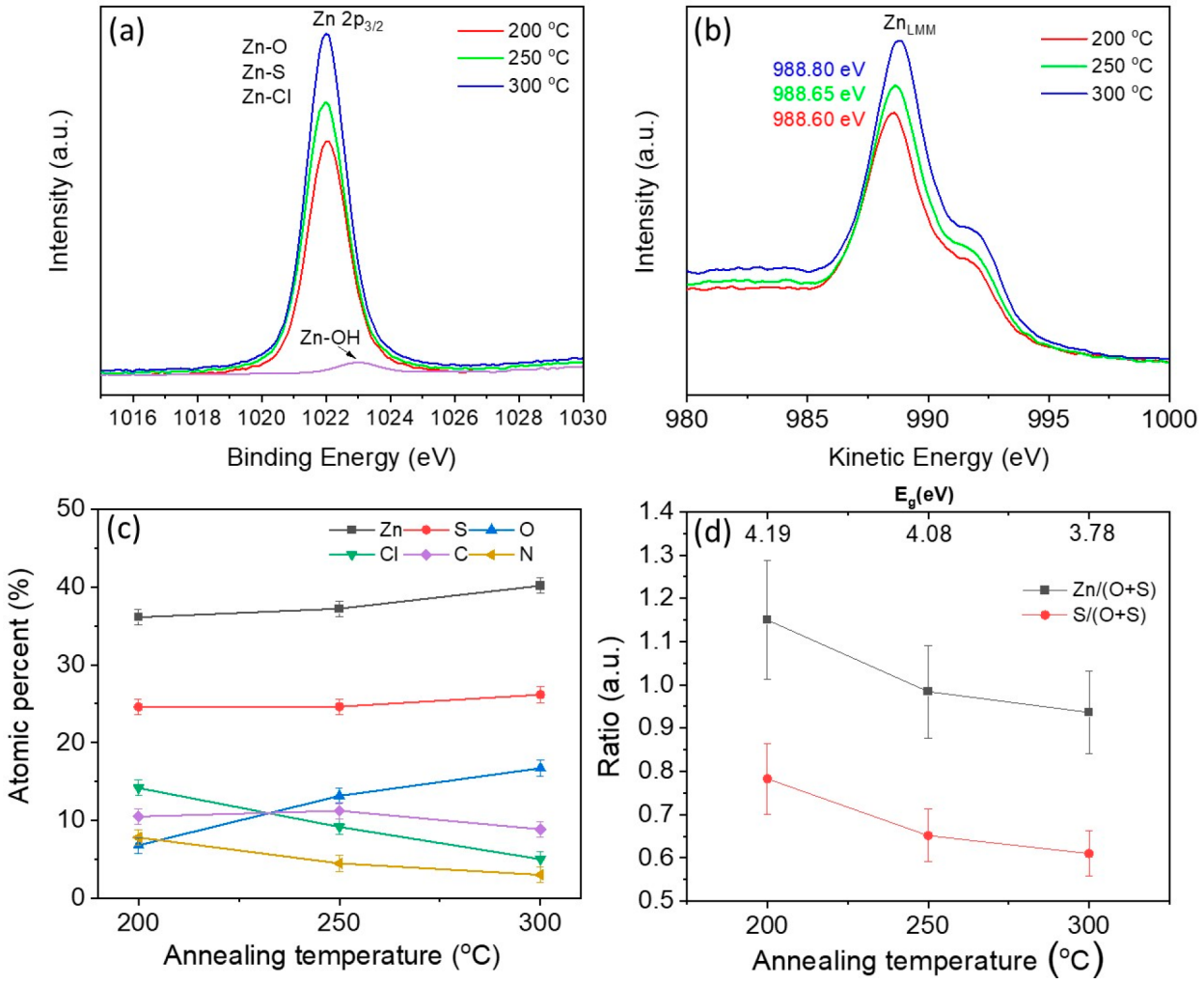

Figure 5. Detailed (a) Zn $2p_{3/2}$ and (b) Zn_{LMM} peaks as well as (c) the average atomic composition and (d) the atomic ratios Zn/(O+S) and S/(O+S) of the Zn(O,S) films annealed at different temperatures determined by X-ray photoelectron spectroscopy.

some of the precursor components. S is the main anion detected in the films, with lesser amounts of oxygen and chlorine, independent of the annealing temperature, confirming the XRD result that Zn is mainly bonded to sulfur. The bonding characteristics of the Zn(O,S) films are investigated by analyzing the binding energy peaks and the Auger parameter, which is the sum of the Zn 2p peak position (binding energy (eV) and Zn LMM Auger peak (kinetic energy (eV)). The Zn $2p_{3/2}$ spectra acquired at the surface of the samples annealed at various temperatures are nearly perfectly aligned and have an identical shape (Figure 5a). The Zn $2p_{3/2}$ peak is not sensitive to the chemical environment changes induced by the ratio evolution between Zn−O, Zn−S, or Zn−Cl bonds in the films. A single peak centered at 1022.0 eV is attributed to Zn^{2+} and includes all these contributions. A second component can be added at 1022.9 eV and is usually

https://dx.doi.org/10.1021/acsami.0c16860
ACS Appl. Mater. Interfaces 2021, 13, 13009−13021

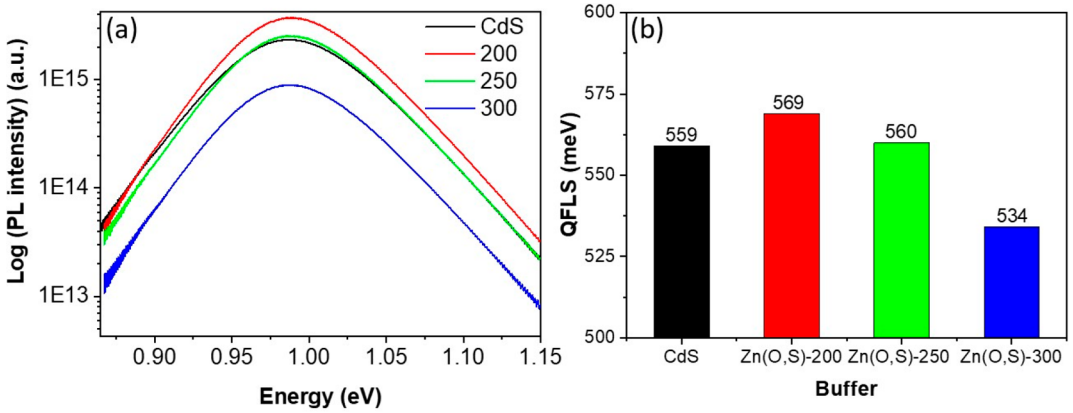

Figure 6. (a) Photoluminescence spectra of CIGS absorbers covered with CdS and Zn(O,S) films annealed at 200, 250, and 300 °C and (b) the corresponding quasi-Fermi level splitting values estimated from the photoluminescence spectra.

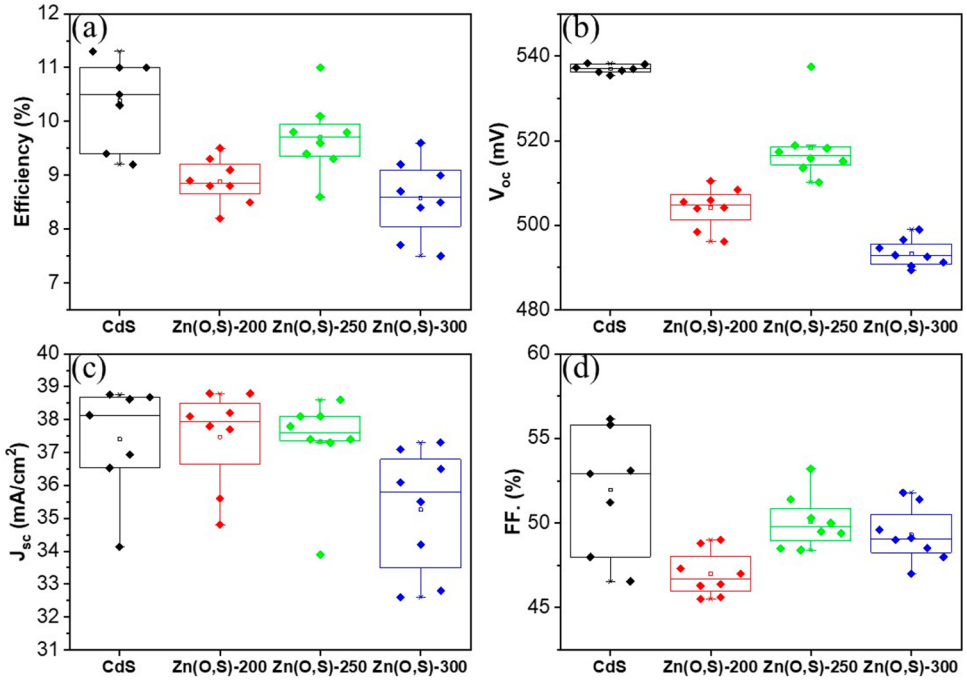

Figure 7. Performance comparison of (a) efficiency, (b) open circuit voltage, (c) current density, and (d) fill factor of CIGS solar cells using inkjet-printed Zn(O,S) films printed with drop spacing of 35 μm and air annealed at 200, 250, and 300 °C and conventional CBD-CdS buffer layers.

attributed to hydroxide components ($Zn(OH)_2$).[50] Interestingly, the Zn_{LMM} peaks show a slight shift toward higher kinetics energy with increasing annealing temperature (Figure 5b). The Auger parameter values thus slightly rise from 2010.6 to 2010.8 eV, placing them between those of pure ZnO (2009.8−2010.25 eV) and pure ZnS (2011.4−2011.7 eV).[50] $ZnCl_2$ has the lowest Auger parameter value (2009.3−2009.7 eV), meaning that the increasing Auger parameter is likely linked with the decrease in the number of Zn−Cl bonds in the film for higher annealing temperatures.[50]

Figure 5c shows the elemental composition of the Zn(O,S) films, measured in the middle of each film, annealed at 200, 250, and 300 °C where the absolute error of the XPS instrument is ±1 at. %. The Zn(O,S) film annealed at 200 °C exhibits less oxygen than chlorine. Higher annealing temperatures relatively increase the Zn and S amounts slightly, whereas the O content increases significantly. In addition, increasing the annealing temperature results in a significant reduction in Cl and N as the decomposition of these precursors and their complexes occurs above 200 °C, as has already been reported.[51,52]

Figure 5d shows the Zn/(O+S) and S/(O+S) ratios. At 200 °C, the S/(S+O) ratio is around 0.8, dropping to around 0.6 at 300 °C. This indicates that the higher-temperature sample contains more oxygen and thus should have a smaller band gap than the low-temperature sample, which is in agreement with the optical measurements. Surprisingly, the increase in oxygen seems not to be at the expense of sulfur, but rather chlorine and/or nitrogen. Within error, the Zn/(O+S) ratio is around one, although just at the edge of the measurement error at 200 °C. Taken altogether, it appears that at 200 °C Zn(O,S) is incompletely formed, and that some of the Zn atoms are bound to Cl.

For photovoltaic applications, the band gap energy and energy alignment of the buffer strongly affects all the performance parameters of solar cells.[53,54] A buffer layer with

https://dx.doi.org/10.1021/acsami.0c16860
ACS Appl. Mater. Interfaces 2021, 13, 13009−13021

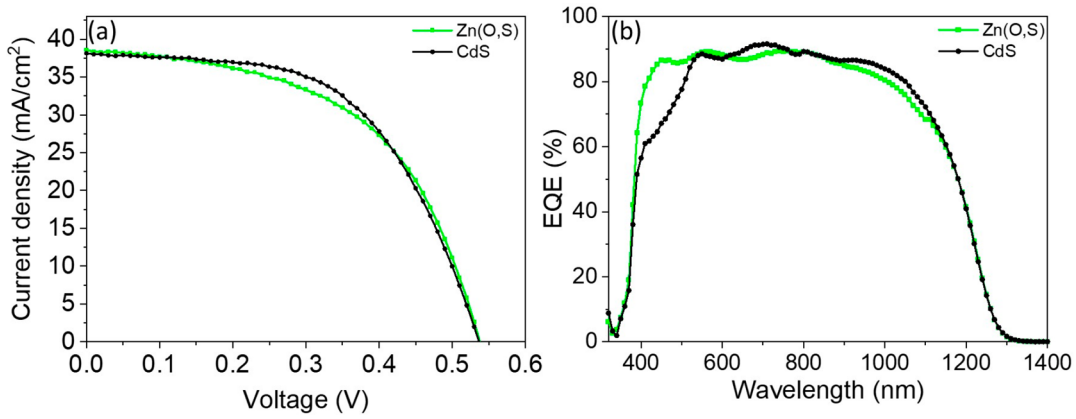

Figure 8. (a) $J-V$ characteristics of the best CIGS solar cells using inkjet-printed Zn(O,S) annealed at 250 °C in air for 10 min and CBD-CdS buffer layers and (b) their external quantum efficiencies.

a wider band gap than the traditional CdS, allows more photons from the Sun to pass through and enter the absorber film, thus generating more charge carriers and increasing the current density of the solar cells. In addition, the band gap of Zn(O,S) films also determines the band energy alignment with the absorber film, and the conduction band offset that helps define the open circuit voltage potential of the solar cell device.[55] To determine the open circuit voltage potential achievable from CIGS solar cells using Zn(O,S) buffers, we printed Zn(O,S) films on CIGS absorber layers and annealed them at different temperatures and investigated their quasi Fermi level splitting (qFLs). The qFLs is calculated from the photoluminescence (PL) spectra of the CIGS coated buffers and is the upper limit for the possible device open circuit voltage.[56,57] Samples were prepared identically except for the three different air annealing temperatures of 200, 250, and 300 °C. For comparison, a standard CdS buffer layer was also deposited by chemical bath on a CIGS absorber at 60 °C and post annealing at 200 °C. Figure 6 shows the photoluminescence spectra (a) and the calculated qFLs (b) of the samples. The qFLs of the Zn(O,S) samples annealed at 200, 250, and 300 °C were 569, 560, and 534 meV, respectively, whereas the qFLs of the CdS sample was 559 meV, which is similar to the two lowest temperature Zn(O,S) films. This shows that the absorber layer is well covered by the Zn(O,S), because bare absorbers that have been air annealed at high temperature normally have significantly lower qFLs, and that the Zn(O,S) CIGS interface does not cause significant recombination. These results show the potential to get similar or even slightly higher open circuit voltages for the solar cells based on inkjet-printed Zn(O,S) thin films than those based on CdS.

We fabricated CIGS thin film solar cells using Zn(O,S) printed with drop spacing of 35 μm and compared the performance with CIGS solar cells using a CBD-CdS buffer layer. Figure 7 shows the performance of eight CIGS solar cells per buffer condition. The average efficiencies of the CIGS solar cells using Zn(O,S) annealed at 200, 250, and 300 °C were 8.9, 9.7 and 8.6%, respectively. The average efficiency of CIGS solar cells using CdS buffer layer was 10.4%. Both types of devices achieved almost the same current density except for the solar cells with Zn(O,S) films annealed at 300 °C which had a lower current. The open circuit voltage of the Zn(O,S) buffer air-annealed devices were all on average 20−40 mV lower than that of the CdS buffer devices but were all at least 100 mV higher than a device made without any buffer layer (see Table S2). This again indicates that 30 s UV ozone treatment is sufficient to ensure that the Zn(O,S) buffer layer covers the CIGS, because otherwise we would expect V_{oc} closer to the device without buffer layer. The 200 °C annealed buffer has a V_{oc} 60 mV less than its measured QFLS, whereas the 250 and 300 °C buffers have V_{oc}'s around 40 mV less. The reason that the 200 °C buffer layers have this greater deficit is related to it having a higher diode factor of 2.1 indicating recombination in the space charge region,[58] whereas the hotter annealed buffers have diode factors around 1.5. All the devices suffer from low fill factors. Analysis of current−voltage−temperature measurements shows that they suffer from a diode current barrier that acts as an internal series resistance (see Figure S4). The solar cells with Zn(O,S) films annealed at 250 °C achieved the highest performance among Zn(O,S) devices, and the best solar cell achieved an efficiency similar to that of the CdS device.

Besides changing the S/(O+S) ratio, different annealing temperatures might change the degree of in-diffusion of elements between the absorber and buffer layers. Most studies report the in-diffusion of Zn into the absorber layer, and also consider it necessary for good device performance.[21,59−61] Platzer-Björkmann et al.[21] find Cu in-diffusion into an ALD-deposited Zn(O,S) buffer layer at 120 °C, whereas Zutter et al.[60] find a Cu depletion in the absorber layer at the interface with sputtered Zn(O,S) but found no Cu in-diffusion into the buffer layer itself, for an annealing temperature of 200 °C. Wi et al.[61] found that annealing sputtered Zn(O,S) at 400 °C also caused Cu depletion and a large Zn diffusion into the absorber layer, which caused a large loss in V_{oc}. Here, we measured the secondary ion mass spectrometry (SIMS) profiles of Zn(O,S) buffer layers on CIGS absorbers annealed between 200 and 300 °C (see Figure S5). We find that Cu does appear to diffuse into the buffer layer, and that Zn in turn diffuses into the absorber layer. However, the degree of diffusion appears similar for all annealing temperatures, which might be expected because the range of temperatures used here is relatively narrow, and the annealing time is short. Given the similar profiles of the main elements, we cannot attribute them to any differences to the measured electrical properties.

Figure 8a shows the $J-V$ characteristics of the best solar cell devices fabricated in the same batch using inkjet-printed Zn(O,S) and CdS buffers. The $J-V$ characteristic parameters are listed in Table 2. The best CIGS solar cell using the

https://dx.doi.org/10.1021/acsami.0c16860
ACS Appl. Mater. Interfaces 2021, 13, 13009−13021

Table 2. *J*−*V* Characteristic Parameters of the Best CIGS Solar Cells Using the Temperature Series Printed Zn(O,S) and CdS Buffer Layers

device	eff. (%)	FF (%)	V_{oc} (mV)	J_{sc} (mA/cm^2)	R_s (Ω cm^2)	R_{sh} (Ω cm^2)	A	J_o (A/cm^2)
Zn(O,S)	11.0	53	537	38.6	1.9	402	1.7	1.3×10^{-7}
CdS	11.4	56	537	38.1	2.4	255	1.5	2.3×10^{-8}

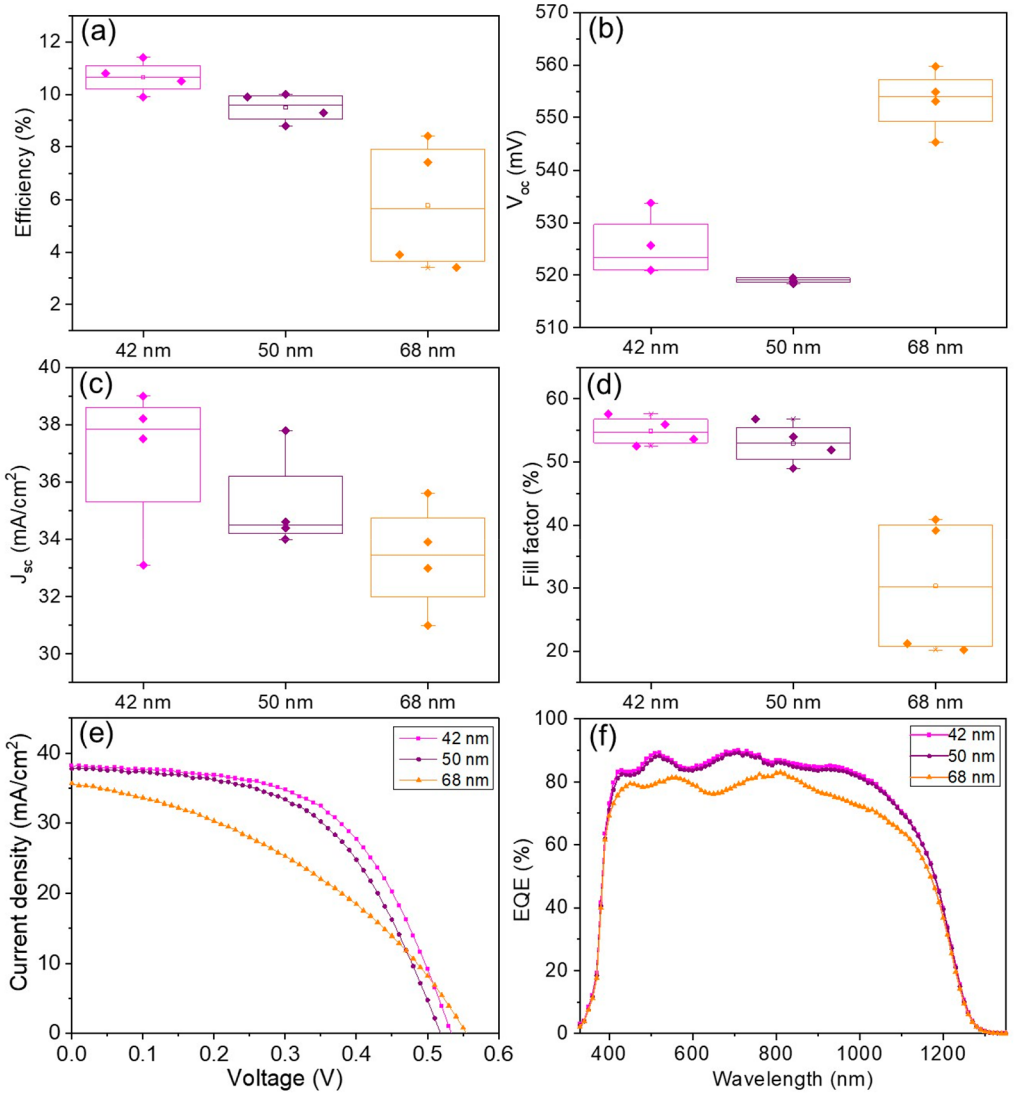

Figure 9. (a−d) Performance of CIGS solar cells using Zn(O,S) film printed with different drop spacing and (e) the *J*−*V* characteristic and (f) the external quantum efficiency of the best solar cell for each thickness.

Zn(O,S) buffer layer achieved an efficiency of 11%, which is similar to the performance of the CdS buffer layer device. Both Zn(O,S) and CdS buffer layer devices obtained an open circuit voltage of 537 mV. The diode quality factor A and the saturation current density J_o of the CdS solar cell are lower than that of the solar cell using Zn(O,S) indicating a better p−n junction formation between n-type CdS and p-type CIGS, resulting in higher fill factor for the CdS buffer layer device. Interestingly, the current density of the solar cell with the Zn(O,S) buffer layer is higher than that of the device using CdS buffer. To understand the improvement in current density for the Zn(O,S) solar cell, we measured the external quantum efficiencies (EQE) of both devices and show them in Figure 8b. The EQE of the Zn(O,S) solar cell demonstrates an enhancement in the blue region compared to that of the CdS buffer layer. By integrating the EQE spectra with respect to the solar spectrum in the wavelength range from 300 to 520 nm for both devices, we calculate that the current density of the Zn(O,S) solar cell is higher by 0.93 mA/cm^2 compared to the CdS cell. This enhancement comes from the larger band gap of Zn(O,S) compared to CdS.

It has been reported that the thickness of the Zn(O,S) buffer layer is a crucial factor for the performance of CIGS thin film solar cells because it affects the charge carrier dynamics.[62] Here, we investigated the effects of the thickness of the inkjet-printed Zn(O,S) thin films on the performance of devices. To vary the thickness of Zn(O,S) films, we tuned the print parameter drop spacing at 25, 30, and 35 μm resulting in the nominal thicknesses of 68, 50, and 42 nm, respectively. We assume the Zn(O,S) thickness is independent of the substrate

https://dx.doi.org/10.1021/acsami.0c16860
ACS Appl. Mater. Interfaces 2021, 13, 13009−13021

Table 3. $J-V$ Characteristic Parameters of CIGS Solar Cells Using Zn(O,S) Buffer Layers Printed with Different Thickness

Zn(O,S) thickness	eff. (%)	FF. (%)	V_{oc} (mV)	J_{sc} (mA/cm^2)	R_s (Ω cm^2)	R_{sh} (Ω cm^2)	A	J_o (A/cm^2)
42 nm	11.4	56	534	38.2	3.5	1853	1.8	2.7×10^{-7}
50 nm	10.6	54	518	37.8	5.7	4300	1.8	5.0×10^{-7}
68 nm	8.0	40	557	35.6	5.9	5800	1.6	1.0×10^{-9}

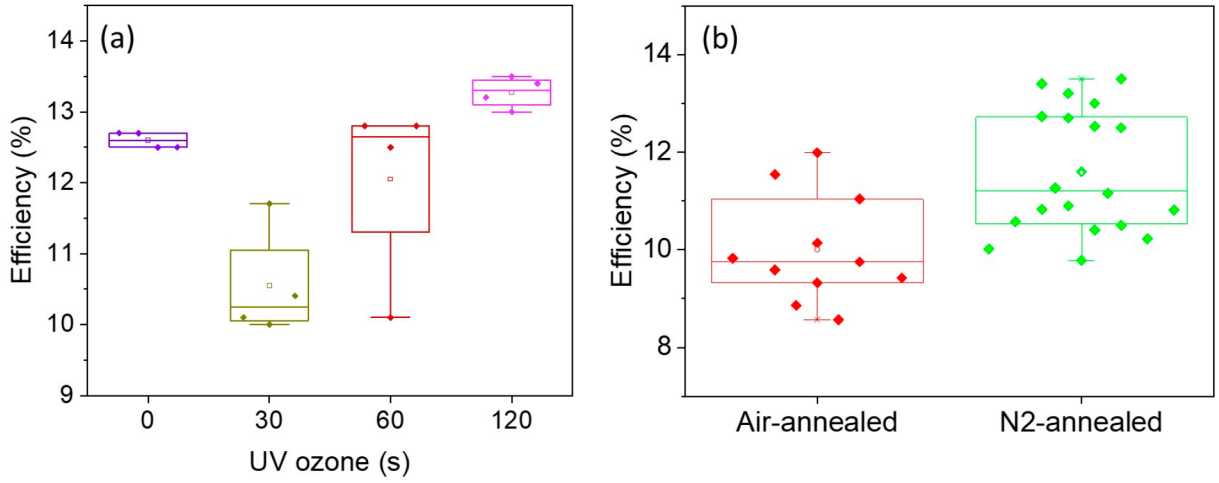

Figure 10. Comparison of power conversion efficiency of solar cells using printed Zn(O,S) buffer on CIGS with (a) different UV ozone treatment times annealed in N_2 at 250 °C and (b) the effect of annealing in air and in a N_2 environment for 120 s of UV ozone treatment.

it is deposited on. Figure 9a–d shows the performance of the solar cells measured under standard 1 Sun conditions. The solar cells with a 42 nm thickness buffer achieved the highest efficiency with the best average current density, whereas the solar cells with a 68 nm thickness buffer achieved a much lower efficiency due to a reduction in the current density and fill factor despite obtaining the highest open circuit voltage. Figure 9e shows the $J-V$ curves of the best solar cell for each thickness with the properties reported in Table 3, and the corresponding external quantum efficiency (EQE) spectra are shown in Figure 9f. The solar cell using the 42 nm buffer achieved the best efficiency of 11.4%, whereas the one using a 68 nm thickness achieved the best efficiency of only 8%. The solar cell with 68 nm Zn(O,S) film has the highest shunt resistance and the lowest saturation current density which leads to obtaining the highest open circuit voltage. However, it exhibits the highest series resistance which strongly suppresses the current density and the fill factor of the solar cells. Reducing the thickness of the Zn(O,S) film results in decreasing the series resistance and consequently obtaining the higher fill factor and current density. The EQEs of the devices with buffer layers of 42 and 50 nm thickness are nearly identical, whereas the device with a thickness of 68 nm shows a lower response over the whole wavelength.

The lower photocurrent response of the device with 68 nm Zn(O,S) compared to the lower thicknesses probably originates from the "spike" conduction band offset at the CIGS/Zn(O,S) interface.[61] A thicker buffer in case of 68 nm Zn(O,S) results in photocurrent blocking effect even at short-circuit conditions.[63,12] To try to confirm this we measured the reverse bias EQE of the 68 nm Zn(O,S) device (see Figure S6). On applying a reverse bias, the whole of the EQE spectra shifts to higher values, which is a sign of photocurrent barrier that can be circumvented by providing sufficient kinetic energy (from applied bias) to the photogenerated carriers. This confirms the presence of a stronger conduction band barrier for the thickest Zn(O,S) buffer layer device.[64]

In an attempt to achieve highly efficient CIGS solar cells, we varied the UV ozone treatment time of the CIGS surface from 0 to 120 s in increments and then directly printed a Zn(O,S) film of 42 nm thickness, as this lowest thickness showed the most promise. The printed Zn(O,S)/CIGS films were then annealed under nitrogen at 250 °C. Figure 10a shows the performance of these devices, which were all fabricated from the same batch of CIGS. The CIGS solar cells using 120 s UV ozone treatment obtained the best performance with an average efficiency of 13.3%, whereas those with lower or no UV ozone treatment had efficiency values of between 10 and 12.5%. It is unclear whether the improvement in efficiency is due to some kind of improved wettability of the Zn(O,S) film so it covers the CIGS surface even more uniformly or if it is due to some changes in the absorber layer such as surface oxidation.[36] Interestingly, the solar cells without UV ozone treatment also showed good performance with an average efficiency of 12.6%. This seems to indicate that the fresh CIGS surface after the KCN etching is wettable enough for the ink to fully cover the surface. In a new separate experiment to try to understand if the annealing atmosphere is important, we compared the performance of the solar cells using the printed Zn(O,S) annealed in nitrogen with those annealed in air at 250 °C. The power conversion efficiency of these devices is shown in Figure 10b and detail on the $J-V$ characteristic is shown in Figure S7. The solar cells annealed in nitrogen achieved higher efficiency with an average of 11.6%, whereas the solar cell annealed in air achieved an average efficiency of 10%. Figure 11 shows the $J-V$ characteristic of the best Zn(O,S) solar cell device and compared with the best reference CdS device. The Zn(O,S) solar cell achieved the best efficiency of 13.5% (Table 4) due to the drastically improved fill factor of 64% while keeping high voltage and high current, compared to all the previous and the CdS reference devices. XPS measurements

https://dx.doi.org/10.1021/acsami.0c16860
ACS Appl. Mater. Interfaces 2021, 13, 13009–13021

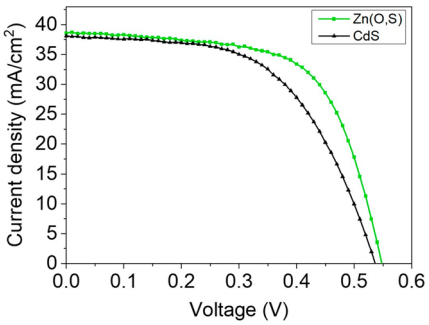

Figure 11. *J*−*V* characteristic of the best CIGS solar cells using 120 s UV-ozone-treated CIGS and printed Zn(O,S) annealed in a N_2 environment at 250 °C for 10 min and the best reference CdS devices.

revealed that the nitrogen-annealed buffer contained slightly more chlorine than the air-annealed buffer layers. Chlorine is a known n -type dopant of ZnO,[65,66] and thus we speculate that this enables the higher V_{oc} that we observe.

CONCLUSION

Nontoxic Zn(O,S) thin films were successfully synthesized by inkjet printing and annealing, consuming 230 000 times less solvent volume and 64 000 times less precursor mass than a conventional chemical bath deposition process. UV ozone treatment of the substrate surface improved the wettability of the ink. The Zn(O,S) films were printed with a drop spacing of 25, 30, and 35 μm forming a continuous layer on the molybdenum substrates with a thickness of 68, 50, and 42 nm, respectively. Grazing-incidence XRD of all the Zn(O,S) films annealed from 200 to 300 °C indicated a cubic structure with a lattice constant close to that of pure ZnS and a nanometer-sized crystal coherence length.

We investigated the optoelectronic properties of Zn(O,S) thin films annealed between 200 and 300 °C and also tested the CIGS solar cells performance using these buffer layers. The optical band gap of the Zn(O,S) films varied from 4.19 to 3.78 eV where the lowest band gap corresponded to the lowest S/(S +O) compositional ratio and the highest annealing temperature. The best air-annealed printed Zn(O,S) CIGS solar cells on average achieved slightly worse efficiencies than those using a CBD-CdS buffer. The CIGS solar cells using printed Zn(O,S) films annealed at 250 °C in air showed better performance with superior open circuit voltage and fill factor than those annealed at higher and lower temperatures. Thinner Zn(O,S) layer devices performed better than thicker layer devices due to a higher short circuit current and fill factor, and a lower series resistance. The thicker Zn(O,S) layer appeared to have an interface barrier at the absorber buffer interface which was reduced in the thinner layers. The solar cells annealed in nitrogen showed better performance than those annealed in air. The highest PCE of 13.5% was achieved with a 120 s UV -zone-treated CIGS film and a 42 nm thickness Zn(O,S) buffer annealed at 250 °C in a nitrogen environment. This study shows that Zn(O,S) buffer layers have successfully formed using a virtually waste free simple inkjet printing and annealing process, and that it could be a good alternative to the toxic CBD-CdS buffer for thin film solar cells.

EXPERIMENTAL SECTION

Ink Preparation. The Zn−S precursor ink is prepared by dissolving $ZnCl_2$ and thiourea $(NH_2)_2C{=}S$) with the Zn:S ratio of 1:1 in distilled water and a mixture of alcohol solution. The total concentration of the precursors in the ink was 0.8 M. First, the $ZnCl_2$ (218 mg, Sigma-Aldrich) was put in a vial containing 1 mL of distilled water, 2 mL of ethanol, and 1 mL of propylene glycol. The solution was stirred for 10 min using a magnetic bar. Then, thiourea (122 mg, Sigma-Aldrich,) was added to the mixture and stirred for 10 min. A clear transparent precursor ink was formed that was ready for inkjet printing.

A prerequisite for a buffer layer in a thin film solar cell is that the layer should cover the absorber surface without pinholes and have a uniform thickness.[67] The ink must suitably jet from the cartridge and wet the surface of the absorber layer to achieve this by inkjet printing. Good jetting occurs with an appropriate solution viscosity, here measured Zn−S ink with an Ostwald viscometer to be 3.5 mPa s at 22 °C for a total ink concentration of 0.8 M. After preparing the ink, it was transferred to a reservoir of the cartridge using a 0.2 μm pore size syringe filter (Whatman, PTFE) to remove any dust particles. On applying a voltage of 20 V to the piezoelectric plates of the inkjet cartridge, ink drops jetted out of the nozzles without clogging.

Inkjet Printing of Zn(O,S) Thin Films. A Dimatix inkjet printer (DMP 2850, Fujifilm) was employed to print the Zn(O,S) thin films. The ink was injected through a 0.2 μm pore syringe filter into the cartridge in order to prevent large residues or dust clogging the nozzles. A 1 pL cartridge was used to print the Zn(O,S) films, meaning the volume of each drop was about 1 pL. A pulse voltage of 20 V was applied to the piezoelectric plates on the cartridge making pressure in the ink reservoir to jet out drops. The drop spacing was varied from 25 to 35 μm to tune the thickness of the Zn(O,S) films. The ink was printed on soda lime glass coated molybdenum, quartz, and silicon wafer substrates. These substrates were ultrasonicated in a 5% decon solution for 10 min and rinsed thoroughly with DI water. The substrates were then ultrasonicated in ethanol for 10 min and dried with a N_2 flow. Finally, the substrates were treated with UV ozone for up to 120 s.

Solar Cell Fabrication. The CIGS absorbers were industrially sourced. In brief, the CIGS films were sputtered on 500 nm Mo-coated glass substrate and post annealed with selenium and sulfur sources. The CIGS films have a Ga/(Ga+In) ratio of less than 0.10 and have a S/(S+Se) ratio of around 0.10. The CIGS films have a band gap of around 1 eV. The thickness of the CIGS films was 2 μm. The CIGS films were etched with a 5% potassium cyanide (KCN) solution for 30 s and dried using N2 flow, and then the CIGS films were pretreated with UV ozone for 30 s unless specified when investigating the effect UV ozone treatment before printing the Zn(O,S) buffer. After printing Zn(O,S) on the CIGS, the films were annealed on a hot plate at 200, 250, or 300 °C for 10 min. The synthesis of comparison CdS buffer layers is as reported elsewhere,[68] except for a subsequent 200 °C annealing on a hot plate in air for 10 min. All devices were completed with sputtered 50 nm intrinsic ZnO and 400 nm Al-doped ZnO window layers deposited at 50 °C followed by e-beam evaporation of the Ni/Al top contact.

Table 4. *J*−*V* Characteristic Parameters of the Best CIGS Solar Cells Using Zn(O,S) Buffer with Pretreatment of CIGS Absorber Using UV Ozone for 120 s and the Printed Zn(O,S) Film Annealed at 250 °C in N_2 for 10 min and the Best Reference CdS Devices

device	eff. (%)	FF (%)	V_{oc} (mV)	J_{sc} (mA/cm^2)	R_s (Ω cm^2)	R_{sh} (Ω cm^2)	A	J_o (A/cm^2)
CdS	11.4	56	537	38.1	2.4	255	1.5	2.3×10^{-8}
Zn(O,S)	13.5	64	548	38.6	2.0	248	1.3	7.5×10^{-9}

https://dx.doi.org/10.1021/acsami.0c16860
ACS Appl. Mater. Interfaces 2021, 13, 13009−13021

Characterization. The formation of the printed Zn(O,S) films with different UV ozone exposure time was examined using an optical microscope (Nikon Eclipse ME600). The morphology and thickness of the films were investigated using a scanning electron microscopy (SEM, Hitachi SU 70) and a profilometer (KLA Tencor P-17). The surface topographic images of the Zn(O,S) films were measured using an atomic force microscope (nanoscope V) under a tapping mode. The reflection and transmission spectra of the Zn(O,S) films on quartz substrates were measured using a UV−vis spectrophotometer (LAMBDA 950) with an integrating sphere. The band gap of the Zn(O,S) films was estimated using a Tauc plot with a direct allowed transition of Zn(O,S) semiconductors $(\alpha h\nu)^2 = A(h\nu - E_g)$, where E_g is the band gap, h is the Planck constant, ν is the frequency of photon, A is a proportional constant, and α is the absorption coefficient, which is determined by $\alpha = \frac{1}{d}\ln\left[\frac{1-R}{T}\right]$, where d is thickness, R is the reflectance,. and T is the transmission of the Zn(O,S) film.[69] The crystal structure of Zn(O,S) films were characterized using grazing-incidence X-ray diffraction (Bruker D8 Discover V2) with the incident angle of 0.5° and the acquisition time was 18 h for each sample. The in-depth composition profile of the Zn(O,S) on CIGS films annealed at different temperature were characterized using a dynamic secondary ion mass spectroscopy (D-SIMS, CAMECA SC Ultra). The photoluminescence (PL) spectra of the Zn(O,S) printed on CIGS films were measured using a home-built system with a 660 nm wavelength laser as the excitation source. The quasi Fermi level splittings (qFLs) were estimated using Planck's generalized law, which describes the PL yield depending on the energy as a function of absorptivity, temperature, and the qFLs.[70] The compositions of the Zn(O,S) film-coated Si substrates were measured using X-ray photoelectron spectroscopy (Axis Ultra DLD) using a monochromated Al k_a X-ray source working at 150 W. To exclude the surface contamination, we sputtered the samples for 120 s with Ar+ ions of 500 eV, corresponding approximately to 5 nm depth from the surface. The current density−voltage (J−V) characteristics of the solar cells were carried out using an AAA solar simulator with a Xenon short-arc lamp, calibrated with a Si and InGaAs reference cells at 25 °C under a 1 SUN (100 mW cm^{-2}) illumination condition. The current density was measured on the active area of solar cells. The series and shunt resistance, the diode quality factor, and the saturation current density were extracted from the dark J−V characteristics. The external quantum efficiency (EQE) spectra were measured with a home-built system employing chopped illumination from a halogen-xenon lamp and a lock-in amplifier to measure the photocurrent. The JVT measurements were performed by mounting the samples in a closed-cycle cryostat under a base pressure below 4×10^{-3} mbar. For measuring the JVT, a cold mirror halogen lamp was used for illumination with an intensity equivalent to 100 mW/cm^2 by adjusting the height of the lamp from the sample.

■ ASSOCIATED CONTENT

Supporting Information

The Supporting Information is available free of charge at https://pubs.acs.org/doi/10.1021/acsami.0c16860.

AFM topography images; GIXRD; table of peak positions, crystallite sizes, and lattice constants; XPS survey spectra; table of J−V characteristic parameters; temperature-dependent J−V characteristics of CIGS solar cells; SIMS profiles; reverse bias EQE; performance comparisons (PDF)

■ AUTHOR INFORMATION

Corresponding Authors

Van Ben Chu − *Department of Physics and Materials Science, University of Luxembourg, Belvaux L-4422, Luxembourg*; Email: chu.vanben@uni.lu

Phillip J. Dale − *Department of Physics and Materials Science, University of Luxembourg, Belvaux L-4422, Luxembourg*; Email: phillip.dale@uni.lu

Authors

Daniel Siopa − *Department of Physics and Materials Science, University of Luxembourg, Belvaux L-4422, Luxembourg*

Alice Debot − *Department of Physics and Materials Science, University of Luxembourg, Belvaux L-4422, Luxembourg*

Damilola Adeleye − *Department of Physics and Materials Science, University of Luxembourg, Belvaux L-4422, Luxembourg*

Mohit Sood − *Department of Physics and Materials Science, University of Luxembourg, Belvaux L-4422, Luxembourg*

Alberto Lomuscio − *Department of Physics and Materials Science, University of Luxembourg, Belvaux L-4422, Luxembourg*; orcid.org/0000-0002-3356-2486

Michele Melchiorre − *Department of Physics and Materials Science, University of Luxembourg, Belvaux L-4422, Luxembourg*

Jérôme Guillot − *Luxembourg Institute of Science and Technology, Materials Research and Technology Department, Belvaux L-4422, Luxembourg*

Nathalie Valle − *Luxembourg Institute of Science and Technology, Materials Research and Technology Department, Belvaux L-4422, Luxembourg*

Brahime El Adib − *Luxembourg Institute of Science and Technology, Materials Research and Technology Department, Belvaux L-4422, Luxembourg*

Jonathan Rommelfangen − *Department of Physics and Materials Science, University of Luxembourg, Belvaux L-4422, Luxembourg*

Complete contact information is available at: https://pubs.acs.org/10.1021/acsami.0c16860

Notes

The authors declare no competing financial interest.

■ ACKNOWLEDGMENTS

This work was supported by Fond National de la Recherche through the STARSOL project (C18/MS/12686759), CORRKEST, AFR Project 13584473, and the MASSENA DTU 10935404, as well as by the University of Luxembourg. Alex Redinger and Susanne Siebentritt are acknowledged for helpful discussions and Lena Merges is acknowledged for sample preparation.

■ REFERENCES

(1) Wu, X. High-Efficiency Polycrystalline CdTe Thin-Film Solar Cells. *Sol. Energy* **2004**, *77*, 803−814.

(2) Sinha, T.; Lilhare, D.; Khare, A. A Review on the Improvement in Performance of CdTe/CdS Thin-Film Solar Cells Through Optimization of Structural Parameters. *J. Mater. Sci.* **2019**, *54*, 12189−12205.

(3) Powalla, M.; Paetel, S.; Hariskos, D.; Wuerz, R.; Kessler, F.; Lechner, P.; Wischmann, W.; Friedlmeier, T. M. Advances in Cost-Efficient Thin-Film Photovoltaics Based on Cu(In,Ga)Se_2. *Engineering* **2017**, *3*, 445−451.

(4) Schock, H. W.; Noufi, R. CIGS-Based Solar Cells for the Next Millennium. *Prog. Photovoltaics* **2000**, *8*, 151.

(5) Abou-Ras, D.; Kostorz, G.; Romeo, A.; Rudmann, D.; Tiwari, A. N. Structural and Chemical Investigations of CBD-and PVD-CdS Buffer Layers and Interfaces in Cu (In, Ga) Se_2-Based Thin Film Solar Cells. *Thin Solid Films* **2005**, *480*, 118−123.

(6) Han, J. F.; Liao, C.; Cha, L. M.; Jiang, T.; Xie, H. M.; Zhao, K.; Besland, M. P. TEM and XPS Studies on CdS/CIGS Interfaces. *J. Phys. Chem. Solids* **2014**, *75*, 1279−1283.
(7) Heske, C.; Eich, D.; Fink, R.; Umbach, E.; van Buuren, T.; Bostedt, C.; Terminello, L. J.; Kakar, S.; Grush, M. M.; Callcott, T. A.; Himpsel, F. J.; Ederer, D. L.; Perera, R. C. C.; Riedl, W.; Karg, F. Observation of Intermixing at the Buried CdS/Cu (In, Ga) Se_2 Thin Film Solar Cell Heterojunction. *Appl. Phys. Lett.* **1999**, *74*, 1451−1453.
(8) Liao, D.; Rockett, A. Cd Doping at the $CuInSe_2$/CdS Heterojunction. *J. Appl. Phys.* **2003**, *93*, 9380−9382.
(9) Hariskos, D.; Spiering, S.; Powalla, M. Buffer Layers in Cu(In,Ga)Se_2 Solar Cells and Modules. *Thin Solid Films* **2005**, *480−481*, 99−109.
(10) Kobayashi, T.; Yamauchi, K.; Nakada, T. Comparison of cell Performance of ZnS(O,OH)/CIGS Solar Cells with UV-Assisted MOCVD-ZnO:B and Sputter-Seposited ZnO:Al Window Layers. *2012 IEEE 38th Photovoltaic Specialists Conference (PVSC) PART 2, Austin, TX* **2012**, 1−6.
(11) Tang, F.-L.; Liu, R.; Xue, H.-T.; Lu, W.-J.; Feng, Y.-D.; Rui, Z.-Y.; Huang, M. Lattice Structures and Electronic Properties of CIGS/CdS Interface: First-Principles Calculations. *Chin. Phys. B* **2014**, *23*, 077301.
(12) Scheer, R.; Schock, H. W. Chalcogenide Photovoltaics: Physics. *Technologies, and Thin Film Devices*; John Wiley & Sons, 2011.
(13) Weinhardt, L.; Fuchs, O.; Groß, D.; Storch, G.; Umbach, E.; Dhere, N. G.; Kadam, A. A.; Kulkarni, S. S.; Heske, C. Band Alignment at the CdS/Cu(In,Ga)S_2 Interface in Thin-Film Solar Cells. *Appl. Phys. Lett.* **2005**, *86*, 062109.
(14) Rana, T. R.; Kim, S. Y.; Kim, J. H.; Kim, K. H.; Yun, J. H. A Cd-Reduced Hybrid Buffer Layer of CdS/Zn(O,S) for Environmentally Friendly CIGS Solar Cells. *Sustain. Energy Fuels* **2017**, *1*, 1981−1990.
(15) Nakamura, M.; Yamaguchi, K.; Kimoto, Y.; Yasaki, Y.; Kato, T.; Sugimoto, H. Cd-Free Cu(In,Ga)$(Se,S)_2$ Thin-Film Solar Cell With Record Efficiency of 23.35%. *IEEE J. Photovolt.* **2019**, *9*, 1863−1867.
(16) Khomyak, V.; Shtepliuk, I.; Khranovskyy, V.; Yakimova, R. Band-Gap Engineering of $ZnO_{1-x}S_x$ Films Grown by rf Magnetron Sputtering of ZnS Target. *Vacuum* **2015**, *121*, 120−124.
(17) Cho, D. H.; Lee, W. J.; Kim, M. E.; Kim, K.; Yun, J. H.; Chung, Y. D. Reactively Sputtered Zn(O,S) Buffer Layers for Controlling Band Alignment of Cu(In,Ga)Se_2 Thin-Film Solar Cell Interface. *J. Alloys Compd.* **2020**, *842*, 155986.
(18) Dwivedi, D.; Patel, T. A.; Panda, E. Simple, Inexpensive Way of Fabricating High Quality Zn(O)S Nanoparticles by Varying pH. *Mater. Sci. Semicond. Process.* **2018**, *79*, 1−6.
(19) Lin, X.; Li, H.; Qu, F.; Gu, H.; Wang, W. Cu(In,Ga)Se_2 Solar Cell with Zn(S,O) as the Buffer Layer Fabricated by a Chemical Bath Deposition Method. *Sol. Energy* **2018**, *171*, 130−141.
(20) Nakada, T.; Mizutani, M. 18% efficiency Cd-Free Cu(In,Ga)Se_2 Thin-Film Solar Cells Fabricated Using Chemical Bath Deposition (CBD)-ZnS buffer layers. *Jpn. J. Appl. Phys.* **2002**, *41*, L165−L167.
(21) Platzer-Björkman, C.; Törndahl, T.; Abou-Ras, D.; Malmström, J.; Kessler, J.; Stolt, L. Zn(O,S) Buffer Layers by Atomic Layer Deposition in Cu(In,Ga)Se_2 Based Thin Film Solar Cells: Band Alignment and Sulfur Gradient. *J. Appl. Phys.* **2006**, *100*, 044506.
(22) Okamoto, A.; Minemoto, T.; Takakura, H. Application of Sputtered $ZnO_{1-x}S_x$ Buffer Layers for Cu(In,Ga)Se_2 Solar Cells. *Jpn. J. Appl. Phys.* **2011**, *50*, 04DP10.
(23) Bacaksiz, E.; Gorur, O.; Tomakin, A.; Yanmaz, E.; Altunbas, A. Ag Diffusion in ZnS Thin Films Prepared by Spray Pyrolysis. *Mater. Lett.* **2007**, *61*, 5239−5242.
(24) Qu, Z. L.; Cheng, X. M.; He, R. J.; Pei, Y. M.; Zhang, R. B.; Fang, D. N. Rapid Heating Thermal Shock Behavior Study of CVD ZnS Infrared Window Material: Numerical and Experimental Study. *J. Alloys Compd.* **2016**, *682*, 565−570.
(25) Bu, I. Y. Y. Sol−gel Synthesis of ZnS (O,OH) Thin Films: Influence of Precursor and Process Temperature on Its Optoelectronic Properties. *J. Lumin.* **2013**, *134*, 423−428.
(26) Mokili, B.; Charreire, Y.; Cortes, R.; Lincot, D. Extended X-Ray Absorption Fine Structure Studies of Zinc Hydroxo-Sulphide Thin Films Chemically Deposited from Aqueous Solution. *Thin Solid Films* **1996**, *288*, 21−28.
(27) Terada, N.; Widodo, R. T.; Itoh, K.; Kong, S. H.; Kashiwabara, H.; Okuda, T.; Obara, K.; Niki, S.; Sakurai, K.; Yamada, A.; Ishizuka, S. Characterization of Interface Nature and Band Alignment in CBD-CdS/Cu(In,Ga)Se_2 bi-Layer Structure by Photoemission and Inverse Photoemission Spectroscopy. *Thin Solid Films* **2005**, *480*, 183−187.
(28) Derby, B. Inkjet Printing of Functional and Structural Materials: Fluid Property Requirements, Feature Stability,and Resolution. *Annu. Rev. Mater. Res.* **2010**, *40*, 395−414.
(29) Marin, V.; Holder, E.; Wienk, M. M.; Tekin, E.; Kozodaev, D.; Schubert, U. S. Ink-Jet Printing of Electron Donor/Acceptor Blends: Towards Bulk Heterojunction Solar Cells. *Macromol. Rapid Commun.* **2005**, *26*, 319−324.
(30) Kuang, M.; Wang, L.; Song, Y. Controllable Printing Droplets for High-Resolution Patterns. *Adv. Mater.* **2014**, *26*, 6950−6958.
(31) Kim, B.; Jang, S.; Geier, M. L.; Prabhumirashi, P. L.; Hersam, M. C.; Dodabalapur, A. Inkjet Printed Circuits on Flexible and Rigid Substrates Based on Ambipolar Carbon Nanotubes with High Operational Stability. *Nano Lett.* **2014**, *14*, 3683−3687.
(32) Hoth, C. N.; Schilinsky, P.; Choulis, S. A.; Brabec, C. J. High-Speed, Inkjet-Printed Carbon Nanotube/Zinc Tin Oxide Hybrid Complementary Ring Oscillators. *Nano Lett.* **2008**, *8*, 2806−2813.
(33) Li, Z.; Li, P.; Chen, G.; Cheng, Y.; Pi, X.; Yu, X.; Yang, D.; Han, L.; Zhang, Y.; Song, Y. Ink Engineering of Inkjet Printing Perovskite. *ACS Appl. Mater. Interfaces* **2020**, *12*, 39082−39091.
(34) Lin, X.; Klenk, R.; Wang, L.; Köhler, T.; Albert, J.; Fiechter, S.; Ennaoui, A.; Lux-Steiner, M. C. 11.3% Efficiency Cu(In,Ga)$(S,Se)_2$ Thin Film Solar Cells: Via drop-on-Demand Inkjet Printing. *Energy Environ. Sci.* **2016**, *9*, 2037−2043.
(35) 35. Lee, Y.-I.; Goo, Y.-S.; Lee, K.-J.; Hwang, Y.-G.; Byun, Y.; Park, H. J.; Park, D.-Y.; Myung, N. V.; Choa, Y.-H. Effect of UV/Ozone Treatment on Interactions Between Ink-jet Printed Cu Patterns and Polyimide Substrates. *Thin Solid Films* **2011**, *519*, 6853−6857.
(36) van Maris, V. R.; Hauschild, D.; Niesen, T. P.; Eraerds, P.; Dalibor, T.; Palm, J.; Blum, M.; Yang, W.; Heske, C.; Weinhardt, L. Impact of UV-Induced Ozone and Low-Energy Ar^+-Ion Cleaning on the Chemical Structure of Cu(In,Ga)$(S,Se)_2$ Absorber Surfaces. *J. Appl. Phys.* **2020**, *128*, 155301.
(37) Regesch, D.; Gütay, L.; Larsen, J. K.; Deprédurand, V.; Tanaka, D.; Aida, Y.; Siebentritt, S. Degradation and Passivation of $CuInSe_2$. *Appl. Phys. Lett.* **2012**, *101*, 112108.
(38) Zhang, S.; Yu, F.; Yuan, Q.; Wang, Y.; Wei, S.; Tesfamichael, T.; Liang, B.; Wang, H. UV-Ozone Induced Surface Passivation to Enhance the Performance of Cu_2ZnSnS_4 Solar Cells. *Sol. Energy Mater. Sol. Cells* **2019**, *200*, 109892.
(39) Ponter, A. B.; Jones, W. R., Jr.; Jansen, R. H. Surface Energy Changes Produced by Ultraviolet-Ozone Irradiation of Poly(methyl Methacrylate), Polycarbonate, and Polytetrafluoroethylene. *Polym. Eng. Sci.* **1994**, *34*, 1233−1238.
(40) Alexander, J. N.; Higashiya, S.; Caskey, D., Jr; Efstathiadis, H.; Haldar, P. Deposition and Characterization of Cadmium Sulfide (CdS) by Chemical Bath Deposition Using an Alternative Chemistry Cadmium Precursor. *Sol. Energy Mater. Sol. Cells* **2014**, *125*, 47−53.
(41) Barange, N.; Chu, V. B.; Nam, M.; Ahn, I. H.; Kim, Y. D.; Han, I. K.; Min, B. K.; Ko, D. H. Ordered Nanoscale Heterojunction Architecture for Enhanced Solution-Based $CuInGaS_2$ Thin Film Solar Cell Performance. *Adv. Energy Mater.* **2016**, *6*, 1601114.
(42) Raleaooa, P. V.; Roodt, A.; Mhlongo, G. G.; Motaung, D. E.; Ntwaeaborwa, O. M. Analysis of the Structure, Particle Morphology and Photoluminescent Properties of ZnS:Mn^{2+} Nanoparticulate Phosphors. *Optik* **2018**, *153*, 31−42.
(43) Soltani, N.; Saion, E.; Hussein, M. Z.; Erfani, M.; Abedini, A.; Bahmanrokh, G.; Navasery, M.; Vaziri, P. Visible Light-Induced Degradation of Methylene Blue in the Presence of Photocatalytic ZnS and CdS Nanoparticles. *Int. J. Mol. Sci.* **2012**, *13*, 12242−12258.

https://dx.doi.org/10.1021/acsami.0c16860
ACS Appl. Mater. Interfaces 2021, 13, 13009−13021

(44) Krunks, M.; Madarász, J.; Leskelä, T.; Mere, A.; Niinistö, L.; Pokol, G. Study of Zinc Thiocarbamide Chloride, a Single-Source Precursor for Zinc Sulfide Thin Films by Spray Pyrolysis. *J. Therm. Anal. Calorim.* **2003**, *72*, 497−506.
(45) Offor, P. O.; Ezekoye, B. A.; Ezekoye, V.; Ezema, J. I. Chemical Spray Pyrolysis Synthesis of Zinc Sulphide (ZnS) Thin Films Via Double Source Precursors. *J. Ovonic Res.* **2015**, *11*, 73−77.
(46) Gautron, E.; Buffière, M.; Harel, S.; Assmann, L.; Arzel, L.; Brohan, L.; Kessler, J.; Barreau, N. Microstructural Characterization of Chemical Bath Deposited and Sputtered Zn(O,S) Buffer Layers. *Thin Solid Films* **2013**, *535*, 175−179.
(47) Pietra, F.; De Trizio, L.; Hoekstra, A. W.; Renaud, N.; Prato, M.; Grozema, F. C.; Baesjou, P. J.; Koole, R.; Manna, L.; Houtepen, A. J. Tuning the Lattice Parameter of In_xZn_yP for Highly Luminescent Lattice-Matched Core/Shell Quantum Dots. *ACS Nano* **2016**, *10*, 4754−4762.
(48) Sadekar, H. K.; Ghule, A. V.; Sharma, R. Bandgap Engineering by Substitution of S by Se in Nanostructured $ZnS_{1-x}Se_x$ thin Films Grown by Soft Chemical Route for Nontoxic Optoelectronic Device Applications. *J. Alloys Compd.* **2011**, *509*, 5525−5531.
(49) Uhm, G. R.; Jang, S. Y.; Jeon, Y. H.; Yoon, H. K.; Seo, H. Optimized Electronic Structure of a $Cu(In,Ga)Se_2$ Solar Cell with Atomic Layer Deposited Zn(O,S) Buffer Layer for High Power Conversion Efficiency. *RSC Adv.* **2014**, *4*, 28111.
(50) Dake, L. S.; Baer, D. R.; Zachara, J. M. Auger Parameter Measurements of Zinc Compounds Relevant to Zinc Transport in the Environment. *Surf. Interface Anal.* **1989**, *14*, 71−75.
(51) Wang, S.; Gao, Q.; Wang, J. Thermodynamic Analysis of Decomposition of Thiourea and Thiourea Oxides. *J. Phys. Chem. B* **2005**, *109*, 17281−17289.
(52) Madarasz, J.; Bombicz, P.; Okuya, M.; Kaneko, S. Thermal Decomposition of Thiourea Complexes of Cu(I), Zn(II), and Sn(II) Chlorides as Precursors for the Spray Pyrolysis Deposition of Sulfide Thin Films. *Solid State Ionics* **2001**, *141*, 439−446.
(53) Schnabel, T.; Seboui, M.; Bauer, A.; Choubrac, L.; Arzel, L.; Harel, S.; Barreau, N.; Ahlswede, E. Evaluation of Different Buffer Materials for Solar Cells with Wide-Gap $Cu_2ZnGeS_xSe_{4-x}$ Absorbers. *RSC Adv.* **2017**, *7*, 40105−40110.
(54) Park, G. S.; Chu, V. B.; Kim, B. W.; Kim, D. W.; Oh, H. S.; Hwang, Y. J.; Min, B. K. Achieving 14.4% Alcohol-Based Solution-Processed $Cu(In,Ga)(S,Se)_2$ Thin Film Solar Cell through Interface Engineering. *ACS Appl. Mater. Interfaces* **2018**, *10*, 9894−9899.
(55) Bhattacharya, R. N.; Contreras, M. A.; Egaas, B.; Noufi, R. N.; Kanevce, A.; Sites, J. R. High Efficiency Thin-Film $CuIn_{1-x}Ga_xSe_2$ Photovoltaic Cells Using a $Cd_{1-x}Zn_xS$ Buffer Layer. *Appl. Phys. Lett.* **2006**, *89*, 253503.
(56) Babbe, F.; Choubrac, L.; Siebentritt, S. The Optical Diode Ideality Factor Enables Fast Screening of Semiconductors for Solar Cells. *Sol. RRL* **2018**, *2*, 1800248.
(57) Lomuscio, A.; Rödel, T.; Schwarz, T.; Gault, B.; Melchiorre, M.; Raabe, D.; Siebentritt, S. Quasi-Fermi-Level Splitting of Cu-Poor and Cu-Rich $CuInS_2$ Absorber Layers. *Phys. Rev. Appl.* **2019**, *11*, 054052.
(58) Malm, U.; Malmstrom, J.; Platzer-Bjorkman, C.; Stolt, L. Determination of Dominant Recombination Paths in $Cu(In,Ga)Se_2$ Thin-Film Solar Cells With ALD−ZnO Buffer Layers. *Thin Solid Films* **2005**, *480*, 208−212.
(59) Witte, W.; Hariskos, D.; Eicke, A.; Menner, R.; Kiowski, O.; Powalla, M. Impact of Annealing on $Cu(In,Ga)Se_2$ Solar Cells with Zn(O,S)/(Zn,Mg)O Buffers. *Thin Solid Films* **2013**, *535*, 180−183.
(60) Zutter, M.; Virtuoso, J.; Anacleto, P.; Yasin, L.; Alves, M.; Madeira, M.; Bondarchuk, O.; Mitra, S.; Fuster Signes, D.; Garcia, J. M.; Briones, F.; Waechter, R.; Kiowski, O.; Hariskos, D.; Colombara, D.; Sadewasser, S. Giant V_{oc} Boost of Low-Temperature Annealed $Cu(In,Ga)Se_2$ with Sputtered Zn(O,S) Buffers. *Phys. Status Solidi RRL* **2019**, *13*, 1900145.
(61) Wi, J. H.; Kim, T. G.; Kim, J. W.; Lee, W. J.; Cho, D. H.; Han, W. S.; Chung, Y. D. Photovoltaic Performance and Interface Behaviors of Cu(In,Ga)Se2 Solar Cells with a Sputtered-Zn(O,S) Buffer Layer by High-Temperature Annealing. *ACS Appl. Mater. Interfaces* **2015**, *7*, 17425−17432.
(62) Sun, J.; Nalla, V.; Nguyen, M.; Ren, Y.; Chiam, S. Y.; Wang, Y.; Tai, K. F.; Zheludev, H.; Sun, N.; Batabyal, S. K.; Wong, L. H. Effect of Zn(O,S) Buffer Layer Thickness on Charge Carrier Relaxation Dynamics of $CuInSe_2$ Solar Cell. *Sol. Energy* **2015**, *115*, 396−404.
(63) Pudov, A. O.; Kanevce, A.; Al-Thani, H. A.; Sites, J. R.; Hasoon, F. S. Secondary Barriers in $CdS−CuIn_{1-x}Ga_xSe_2$ Solar Cells. *J. Appl. Phys.* **2005**, *97*, 064901.
(64) Hegedus, S. S.; Shafarman, W. N. Thin-Film Solar Cells: Device Measurements and Analysis. *Prog. Photovoltaics* **2004**, *12*, 155−176.
(65) Tsin, F.; Venerosy, A.; Vidal, J.; Collin, S.; Clatot, J.; Lombez, L.; Paire, M.; Borensztajn, S.; Broussillou, C.; Grand, P. P.; Jaime, S.; Lincot, D.; Rousset, J. Electrodeposition of ZnO window Layer for an All-Atmospheric Fabrication Process of Chalcogenide Solar Cell. *Sci. Rep.* **2015**, *5*, 8961.
(66) Rousset, J.; Saucedo, E.; Herz, K.; Lincot, D. High Efficiency CIGS Based Solar Cells with Electrodeposited ZnO:Cl as Transparent Conducting Oxide Front Contact. *Prog. Photovoltaics* **2011**, *19*, 537−546.
(67) Yeh, T. H.; Hsu, C. H.; Ho, W. H.; Wei, S. Y.; Cai, C. H.; Lai, C. H. An Ammonia-Free Chemical-Bath-Deposited ZnS(O,OH) Buffer Layer for Flexible $Cu(In,Ga)Se_2$ Solar Cell Application: an Eco-Friendly Approach to Achieving Improved Stability. *Green Chem.* **2016**, *18*, 5212−5218.
(68) Werner, F.; Babbe, F.; Burkhart, J.; Spindler, C.; Elanzeery, H.; Siebentritt, S. Interdiffusion and Doping Gradients at the Buffer/Absorber Interface in Thin-Film Solar Cells. *ACS Appl. Mater. Interfaces* **2018**, *10*, 28553−28565.
(69) Raciti, R.; Bahariqushchi, R.; Summonte, C.; Aydinli, A.; Terrasi, A.; Mirabella, S. Optical Bandgap of Semiconductor Nanostructures: Methods for Experimental Data Analysis. *J. Appl. Phys.* **2017**, *121*, 234304.
(70) Wurfel, P. The Chemical Potential of Radiation. *J. Phys. C: Solid State Phys.* **1982**, *15*, 3967.

https://dx.doi.org/10.1021/acsami.0c16860
ACS Appl. Mater. Interfaces 2021, 13, 13009−13021